JOURNAL OF AIRCRAFT
Vol. 44, No. 4, July–August 2007

Computational Fluid Dynamics Study of Three-Dimensional Dynamic Stall of Various Planform Shapes

A. Spentzos,* G. N. Barakos,† K. J. Badcock,‡ B. E. Richards,§ F. N. Coton,¶ and R. A. McD. Galbraith¶
University of Glasgow, Glasgow, G12 8QQ Scotland, United Kingdom
and
E. Berton** and D. Favier††
Laboratoire d'Aérodynamique et de Biomécanique du Mouvement, 13288 Marseille Cedex 9, France

DOI: 10.2514/1.24331

Numerical simulation of 3-D dynamic stall has been undertaken using computational fluid dynamics. As a first step, validation calculations have been performed for cases in which experimental data were available. Although the amount and quality of the experimental data available for 3-D dynamic stall does not match what is available for 2-D cases, the computational fluid dynamics was found capable of predicting this complex 3-D flow with good accuracy. Once confidence on the computational fluid dynamics method was established, further calculations were conducted for several wing planforms. The calculations revealed the detailed structure of the 3-D dynamic stall vortex and its interaction with the tip vortex. Remarkably, strong similarities in the flow topology were identified for wings of very different planforms.

Nomenclature

C_L	=	lift coefficient, $L/(2S\rho U_\infty^2)$
C_p	=	pressure coefficient, $(p - p_\infty)/(2\rho U_\infty^2)$
c	=	chord length of the aerofoil
d	=	distance along the normal to chord direction
k	=	reduced frequency of oscillation, $\omega c/(2U_\infty)$
L	=	lift force
p	=	pressure
Re	=	Reynolds number, $\rho U_\infty c/\mu$
S	=	planform area
t	=	nondimensional time
U_∞	=	freestream velocity
u	=	local streamwise velocity
x, y, z	=	coordinate directions
α	=	instantaneous incidence angle
α_0	=	mean incidence angle for oscillatory cases
α_1	=	amplitude of oscillation
α^+	=	nondimensional pitch rate, $\dot{\alpha}c/U_\infty$
$\dot{\alpha}$	=	pitch rate
μ	=	dynamic viscosity
ρ	=	density
ρ_∞	=	density at freestream
ϕ	=	phase angle
ω	=	angular frequency

Presented as Paper 2005-1107 at the 43rd AIAA Aerospace Sciences Meeting and Exhibit, Reno, NV, 10–13 January 2005; received 29 March 2006; revision received 7 August 2006; accepted for publication 7 August 2006.

*Postgraduate Student, CFD Laboratory, Department of Aerospace Engineering.
†Senior Lecturer, CFD Laboratory, Department of Aerospace Engineering; currently Department of Engineering, University of Liverpool, Liverpool, L69 3GH England, U.K.; g.barakos@liverpool.ac.uk (Corresponding Author).
‡Reader, CFD Laboratory, Department of Aerospace Engineering.
§Professor, CFD Laboratory, Department of Aerospace Engineering.
¶Professor, Low Speed Aerodynamics Group, Department of Aerospace Engineering.
**Professor.
††Research Director.

I. Introduction

THE phenomenon of dynamic stall (DS) is central in rotorcraft aerodynamics and has so far been investigated by various authors. A review up to 1996 of all computational fluid dynamics (CFD) efforts related to DS has been provided by Ekaterinaris et al. [1] and Ekaterinaris and Platzer [2]. Since then, several papers on DS have appeared in the literature [3] and the reader could consult the recent paper by Barakos and Drikakis [4] for an update. A literature survey indicated that since 1995 only three CFD investigations attempted to make the step from 2-D to 3-D simulation of DS with little evidence of success. Newsome [5] focused on the laminar flow regime and attempted to simulate the experiments of Schreck and Helin [6]. Newsome's work predicted the 3-D dynamic stall vortex (DSV) but provided very little information regarding the interaction of this vortex with the tip vortex of the wing. This interaction, as we will show in this work, is important. The work by Morgan and Visbal [7] considered the oscillatory motion of a square wing at laminar flow conditions with end plates at both tips. The objective was to approximate the conditions inside a wind tunnel with the model spanning the test section and was focused on the development of vorticity near the wing surface. The work of Ekaterinaris [8] is the most recent in 3-D DS but to a great extend deals with 2-D configurations, and the 3-D problem is provided as a demonstration of the capabilities of CFD.

Regardless of the lack of CFD investigations, experimental works on 3-D DS were more successful. Table 1 provides a summary of all works the authors have identified in the literature, along with the flow conditions, measured quantities, and experimental techniques. One cannot fail to notice that pressure measurements dominate, whereas flow visualization and velocity profile measurements are rare. In addition, no measurements have been conducted for high aspect ratio (AR) wings or twisted wings, and data for DS of rotating blades are inexistent. It is evident from Table 1 that all experimental effort is so far devoted to the study of the fundamental unsteady aerodynamics problem of DS.

In the present work two objectives have been set: 1) to validate a CFD method for 3-D DS and 2) to investigate the flow topology during the evolution of 3-D DS over various wing planforms. The

Table 1 Summary of experimental investigations for 3-D DS

Case	Reference	Conditions	Measurements
1	Moir and Coton [9]	Ramping and oscillatory motions $Re = 13,000$, $M = 0.1$ NACA0015, AR = 3	Smoke visualization
2	Coton and Galbraith [10]	Ramping and oscillatory motions $Re = 1.5 \times 10^6$, $M = 0.1$ NACA0015, AR = 3	Surface pressure
3	Berton et al. [11]	Oscillatory motion $Re = 3$–6×10^6, $M = 0.01$–0.3 NACA0012	Boundary layers Velocity profiles Turbulence quantities
4	Piziali [12]	Ramping and oscillatory motion $Re = 2.0 \times 10^6$, $M = 0.278$ NACA0015, AR = 10	Surface pressure Flow visualization (micro-tufts)
5	Schreck and Helin [6]	Ramping motion $Re = 6.9 \times 10^4$, $M = 0.03$ NACA0015, AR = 2	Surface pressure Flow visualization (dye injection)
6	Tang and Dowell [13]	Oscillatory motion $Re = 0.52 \times 10^6$, $M = 0.1$	Surface pressure

Table 2 Details of the employed CFD grids

Case	Blocks	Points on wing	Points on tip	Farfield	Wall distance	Topology
1	40	6,750	1,800	8 chords	10^{-5} chords	3-D C-extruded
2a	20	3,375	1,800	8 chords	10^{-5} chords	3-D C-extruded
2b	20	3,375	1,800	8 chords	10^{-5} chords	3-D C-extruded
2c	20	3,375	7,200	8 chords	10^{-5} chords	3-D C-extruded
3	36	7,800	7,200	8 chords	10^{-5} chords	3-D C-extruded
4	28	7,800	7,200	8 chords	10^{-5} chords	3-D C-extruded
5	36	10,800	2,800	8 chords	10^{-4} chords	3-D C-extruded
High AR twisted wing						

paper is organized as follows: A brief description of the method is first presented, which is followed by a description of four selected validation cases. For each case, the original experimental data have been obtained and effort has been made to simulate the experiment as accurately as possible. The experiments and the CFD results are postprocessed and presented in exactly the same way to facilitate comparisons. The validation cases are complemented with an additional case of a high aspect ratio twisted wing, which better approximates a real helicopter blade. After this analysis, the flow topology during 3-D DS is investigated and detailed. Finally, conclusions are drawn and suggestions are put forward for future work.

II. Numerical Method

The employed CFD solver is capable of solving flow conditions from inviscid to fully turbulent using the Reynolds-averaged Navier–Stokes (RANS) equations in three dimensions [14]. Detached eddy simulation and large eddy simulation options are also available. For this work, however, two-equation eddy-viscosity turbulence models have been employed, and most of the presented results have been obtained using the baseline k–ω model [15]. To solve the RANS equations, multiblock grids were generated around the required geometries, and the equations were discretized using the cell-centered finite volume approach. For the discretization of the convective fluxes, Osher's scheme has been used and a formally third-order accurate scheme (on uniform grids) is achieved using a MUSCL interpolation technique. Viscous fluxes were discretized using central differences. Boundary conditions were set using two layers of halo cells, and the solution was marched in time using an implicit second-order scheme. The final system of algebraic equations was solved using a preconditioned Krylov subspace method.

For this work, multiblock structured grids have been used and care has been taken in accurately representing the tip shape of each wing considered. As explained in [16,17], flat wing tips cannot be accurately represented with single-block grids, and several multiblock topologies have been assessed to ensure that the quality of the CFD grids is adequate and the geometry of the wing is represented exactly. Regarding turbulence modeling, no explicit effort has been put to investigate its role in 3-D DS because this would merit a separate investigation. However, laminar cases have been conducted wherever possible, and all turbulent cases have been selected so that Reynolds number is high and therefore transition modeling is of secondary importance.

III. Validation Cases

At present, four validation cases have been selected for computations, out of the experimental investigations presented in Table 1. The first case concerns the flow visualization experiments conducted by Moir and Coton [9] at the smoke tunnel of the University of Glasgow. The second validation case was based on the experiments conducted at the S1L wind tunnel of the University of Marseille and are detailed in [11,18]. The third validation case was based on the experiments by Coton and Galbraith [10] conducted at the Handley–Page wind tunnel of the University of Glasgow, whereas the fourth validation case corresponds to the experiments by Piziali [12].

A summary of the flow conditions of all validation cases along with the quantities measured during the experiments is presented in Table 1. The cases were selected so that a wide range of conditions is covered, including laminar and turbulent flow, oscillating and

Table 3 Details of the CPU time required for calculations; all calculations were performed on a Linux Beowulf cluster with 2.5 GHz Pentium-4 nodes

Case	Size (nodes)	No of processors	CPU time, s
1	2,268,000	12	1.06×10^5
2a ramping	1,134,000	9	2.3×10^5
2b oscillatory	1,134,000	9	7.9×10^5
2c ramping	1,134,000	9	2.3×10^5
3	1,828,000	8	1.15×10^6
4	2,632,000	16	1.15×10^6
5 high AR twisted wing	2,745,432	16	6×10^5

a) Moir and Coton [9] and Coton and Galbraith [10] (left), and Coton and Galbraith [10] swept wing (right). Both use a NACA 0015 section

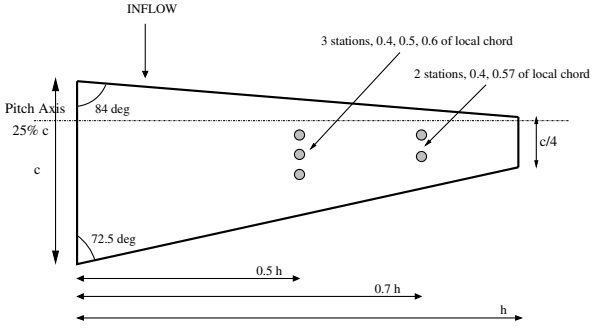

b) Berton *et al.*[11] (NACA 0012 wing section)

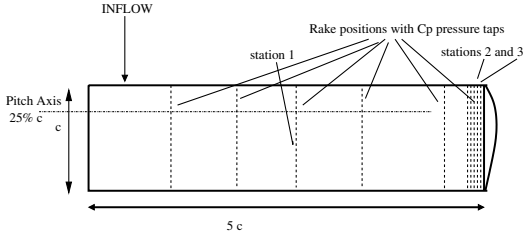

c) Piziali [12] (NACA 0015 wing section)

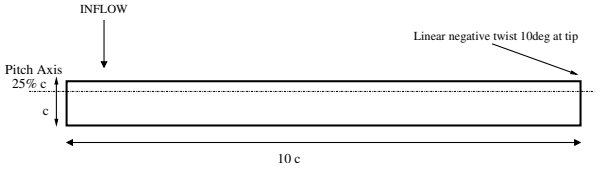

d) High aspect ratio wing (NACA 0015 wing section)

Fig. 1 Wing planforms employed for calculations: a) cases 1 and 2 of Table 1, b) case 3 of Table 1 , c) case 4 of Table 1, and d) wing with linear twist of −10 deg.

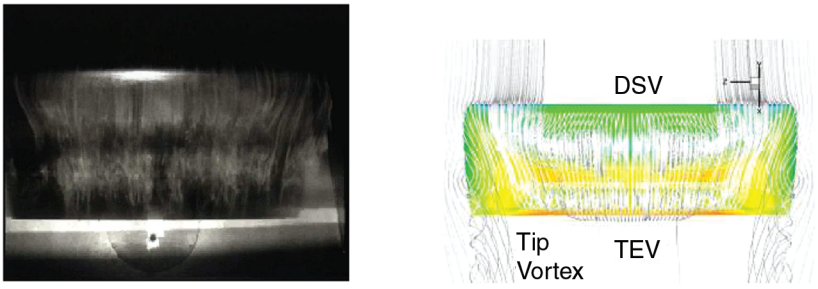

a) Plean view

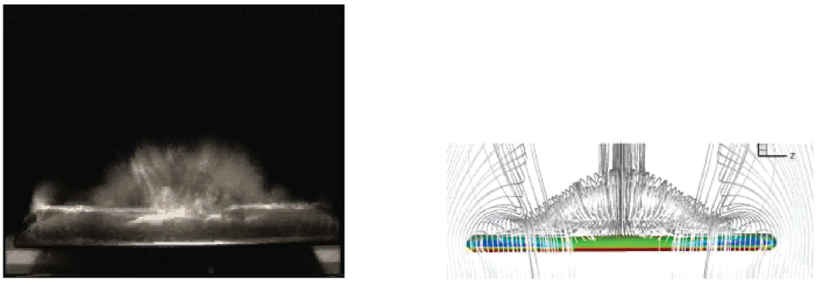

b) View from the leading edge at an incidence angle of 30 deg

Fig. 2 Smoke visualization by Moir and Coton [9] (left) and CFD predictions (right) for the short aspect ratio wing of case 3 of Table 1. Ramping motion between 0 and 40 deg, $Re = 13,000$, $M = 0.1$, $\alpha^+ = 0.16$.

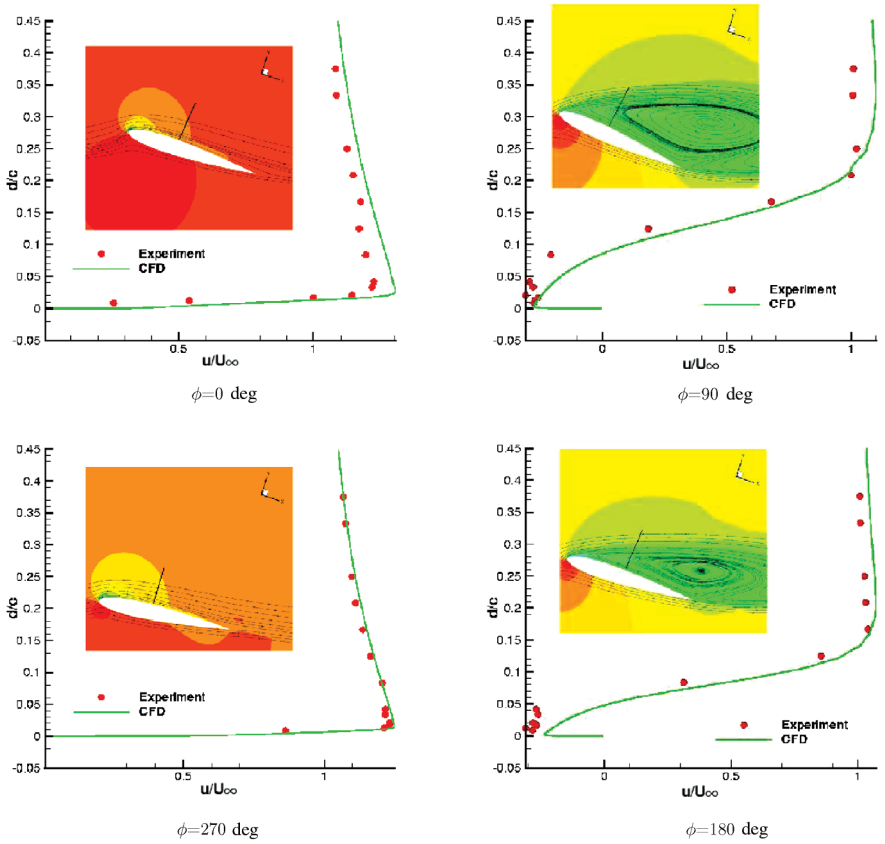

Fig. 3 Comparison between CFD and ELDV measurements by Berton et al. [11] for the u-velocity profiles during DS. Oscillatory motion of a tapered wing, $\alpha(t) = 12 + 6\sin(kt)$ deg, $k = 0.06$, $Re = 10^6$, $M = 0.2$. The line on the inserted plot corresponds to the direction of the ELDV probing, superimposed on pressure contours. The profiles were extracted at a chordwise station of $x/c = 0.4$ and spanwise station of $z/c = 0.5$ (see Fig. 1b).

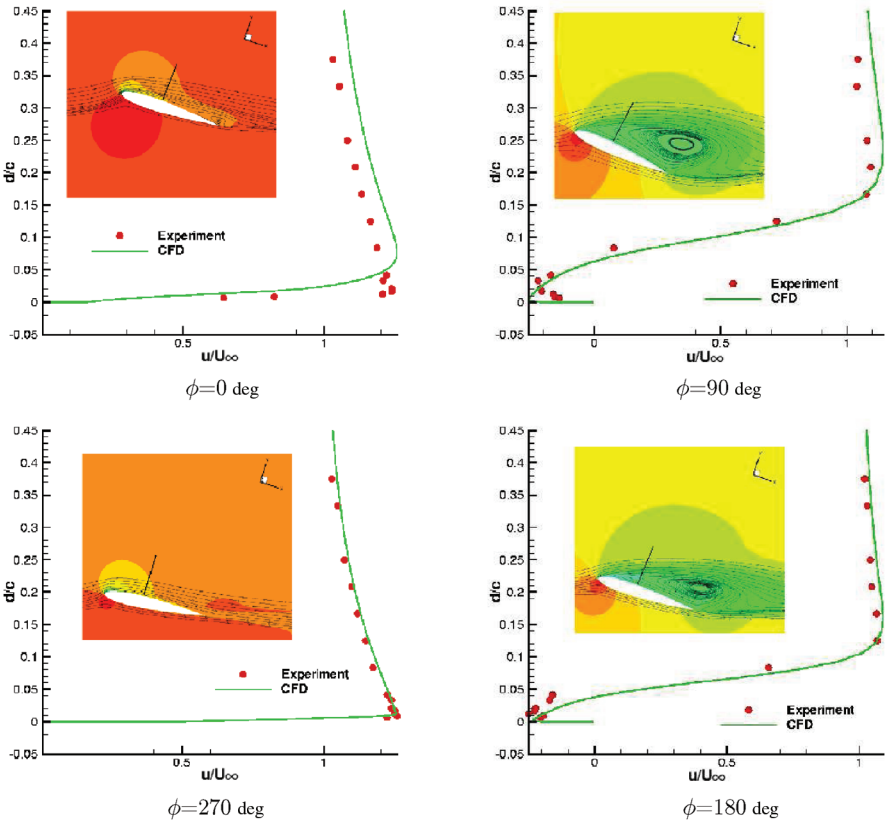

Fig. 4 Comparison between CFD and ELDV measurements by Berton et al. [11] for the u-velocity profiles during DS. Oscillatory motion of a tapered wing, $\alpha(t) = 12 + 6\sin(kt)$ deg, $k = 0.06$, $Re = 10^6$, $M = 0.2$. The line on the inserted plot corresponds to the direction of the ELDV probing, superimposed on pressure contours. The profiles were extracted at a chordwise station of $x/c = 0.4$ and spanwise station of $z/c = 0.7$ (see Fig. 1b).

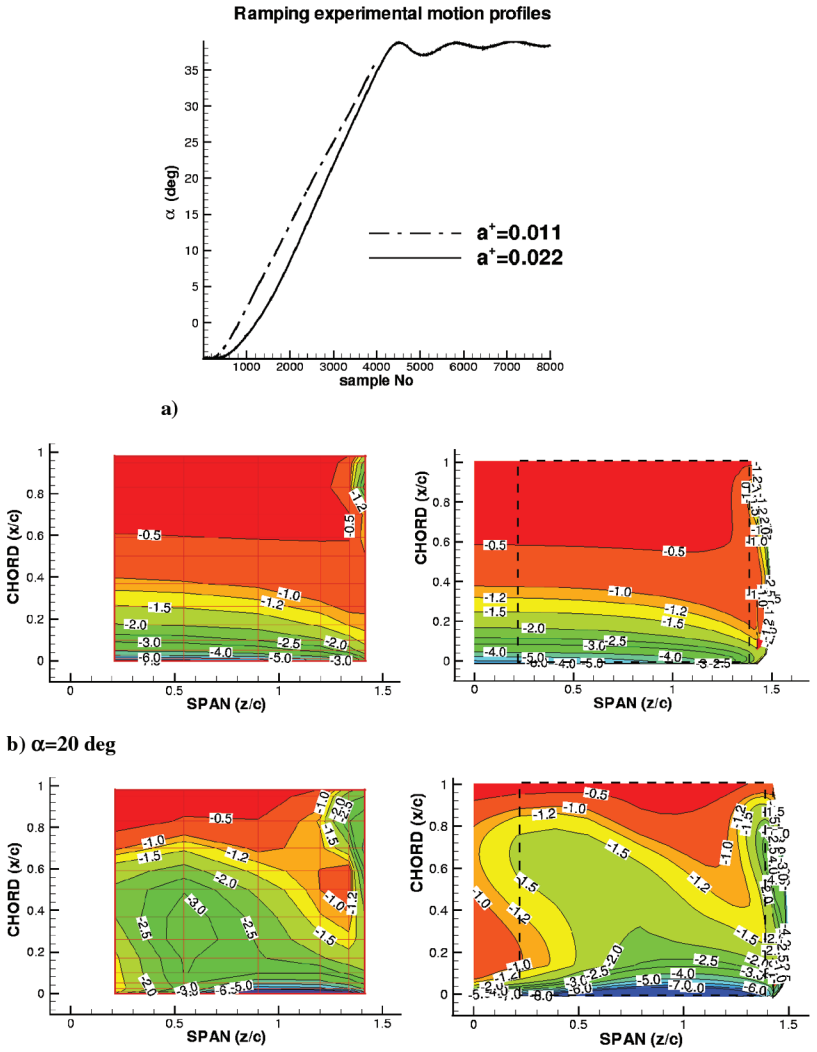

Fig. 5 a) Geometric angle vs sample number of the wing motion for the case by Coton and Galbraith [10] Ramping cases at $\alpha^+ = 0.011$ and $\alpha^+ = 0.022$. b–c) Comparison between experimental (left) and CFD (right) surface pressure distributions for case 4 of Table 1. Ramping wing motion between −5 and 39 deg, $\alpha^+ = 0.022$, $Re = 1.5 \times 10^6$, $M = 0.16$.

ramping wing motions, and several planforms. In addition to the aforementioned cases, CFD calculations have also been undertaken for a fifth planform, although for this last case no experimental data are available. In contrast to the previous cases in which untwisted short aspect ratio wings have been employed, the fourth case dealt with a high aspect ratio twisted wing, which approximates a helicopter rotor blade. For all selected cases, the details of the employed CFD grids along with the CPU time required for computations are presented in Tables 2 and 3, respectively.

Grid and time convergence investigations have been undertaken and the presented results correspond to the largest grids and smallest timesteps. Amongst all cases listed in Table 1, case 6 was left out from the present investigation, because the Reynolds number selected by the experimentalists lies within the transition modeling sensitive regime, as explained in the preceding paragraph. The low Reynolds number case by Schreck and Helin [6] has been presented in a recent paper [16].

A. Flow Visualization Experiments by Moir and Coton [9]

The flow visualization experiments by Moir and Coton [9] provided a detailed account of the initiation and evolution of the DS

Table 4 Fourier expansion coefficients for the two oscillating cases by Coton and Galbraith [10]

$k = 0.092$, $\alpha_o = 0.169892$			$k = 0.17$, $\alpha_o = 0.155459$		
i	α_i	β_i	i	α_i	β_i
1	−0.0717488	0.157438	1	−0.101697	0.125778
2	−0.00809223	−0.00194330	2	0.0161334	−0.0129037
3	−0.00416931	0.00219548	3	0.00914202	−0.000836860
4	−0.00230814	0.000897672	4	−0.00169119	−0.00164984
5	0.001161	−0.00197636	5	−0.000486481	−0.00231397
6	−1.61438E − 05	0.000977314	6	0.000773430	0.000218741
7	0.000539150	0.000387543	7	−0.000166552	−0.000135753
8	3.0956E − 05	−0.000113408	8	0.000357502	−0.000478472
9	−0.000122833	−0.00037934	9	1.5609E − 05	−1.08930E − 05
10	−0.000159201	−6.75040E − 05	10	6.5348E − 05	−0.000338885

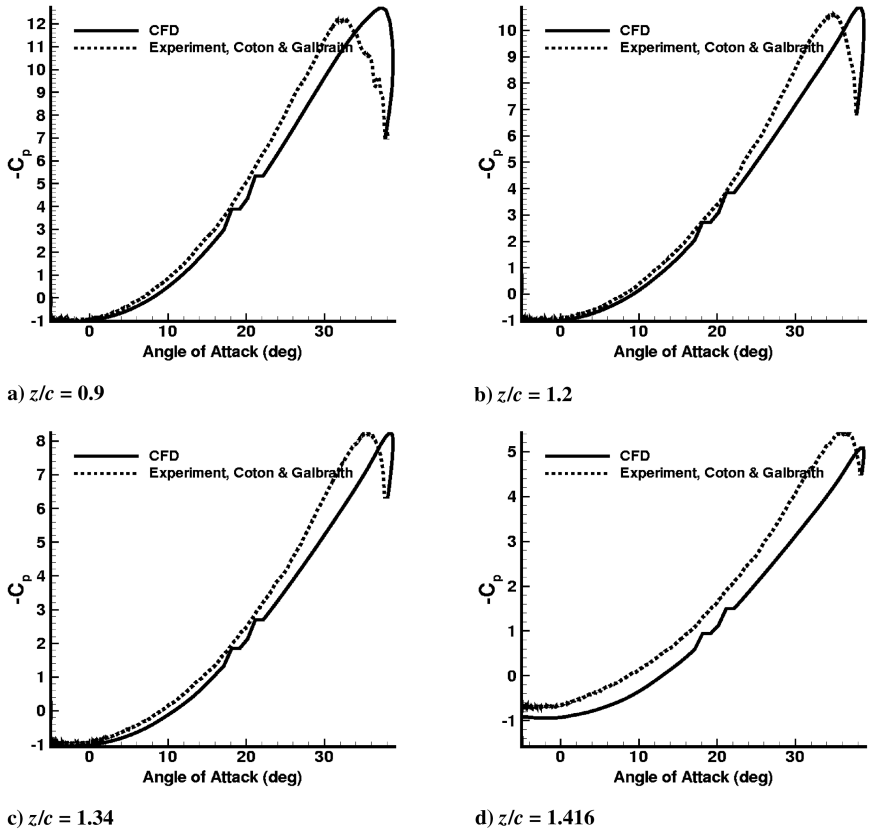

Fig. 6 C_p **vs angle of attack for a single rake of pressure transducers at** $x/c = 0.00025$ **for the ramping case with** $\alpha^+ = 0.022$, $Re = 1.5M$, $M = 0.16$, $M = 0.16$, $\alpha = -5$–40 **deg.**

vortex at laminar flow conditions ($Re = 13,000$). The employed wing was based on the NACA 0015 section and was of rectangular planform with rounded tips and of an aspect ratio of 3. A schematic is shown in Fig. 1a.

CFD calculations have been performed for a ramping case, at a reduced ramping rate of $\alpha^+ = 0.16$, which corresponds to the test conditions used by Moir and Coton [9].

The low Reynolds number of this experiment was beneficial because smoke visualization can be made clearer at lower wind speeds, and from the point of view of CFD no turbulence modeling was necessary. A set of still images has been extracted from the video tapes recorded during the experiments and was consequently used for comparisons with the CFD simulation. Figure 2 presents the comparison between experiments and simulation at incidence angles where, as perceived by the authors, the most important features of the 3-D DS are shown. Figure 2a shows the plan view of the wing at an incidence angle of 30 deg. At this stage, the DSV is well formed and its inboard portion is located at approximately $1/3$ of chord from the leading edge, running parallel to the pitch axis of the wing. The portion, however, of the DSV close to the tips, is deflected towards the leading edge, and appears to interact with the tip vortices. Further aft, one can also see the trailing-edge vortex (TEV), whose ends tend to merge with the DSV and the tip vortices. At this stage, the trailing-edge vortex is of comparable size with the DSV.

Figure 2b shows the same time instance from a different viewing angle, to show the merging of the DSV with the tip vortices, as well as the backwards tilted archlike shape of the DSV resembling that of an inclined Ω. One can see that the streamlines closer to the surface of the wing have the same pattern as the smoke streaks of the visualization. This points to the fact that the DSV impinges on the surface of the wing at a distance of a chord length inboard from the tips in the spanwise direction, and at half a chord's length in the chordwise direction. The trailing-edge vortex can no longer be seen and the flow is dominated by the DSV, which is constantly fed with momentum by the freestream and the wing motion.

B. ELDV Measurements by Berton et al. [11,18]

The DS of an oscillating, tapered, low-aspect-ratio wing has been studied by Berton et al. [11,18]. This is a very interesting case for two reasons: 1) velocity data have been obtained at various phase angles during the oscillation and at several spanwise and chordwise locations, and 2) the wing planform represents an idealization of an active control surface similar to the ones encountered in modern supermaneuverable aircraft.

The experiments [11] were conducted in the S1L high subsonic wind tunnel of the Aerodynamics Laboratory of Marseille, using a novel embedded laser Doppler velocimetry (ELDV) technique. According to this method the laser probe was mounted on the same circular rotating disc that also supported the wing [11,18]. The shape and dimensions of this planform can be seen in Fig. 1b. The employed wing had a root chord length of 0.24 m and was mounted in the wind tunnel's octagonal cross section, which was of a width equal to 3 m. For the cases selected here the freestream velocity was 62.5 m/s. Experimental results [18] are available for oscillatory motion of the wing for several mean angles, amplitudes of oscillation between 3 and 6 deg, and reduced frequencies in the range of 0.02 to 0.1. Two cases were computed, both having a mean angle $\alpha_o = 18$ deg and amplitude $\Delta\alpha = 6$ deg, whereas the reduced frequencies considered were $k = 0.048$ and 0.06.

Comparisons of u-velocity profiles at four different phase angles during the oscillation cycle can be seen in Figs. 3 and 4 for $k = 0.06$; results obtained for the $k = 0.048$ case are not shown. Overall, CFD was found to be in excellent agreement with the experimental data. In each of these figures, one can see an embedded plot of the cross spanwise section where the probing station is also shown. The chordwise location of the probe as well as pressure contours are presented at the corresponding phase angle. For each of the two reduced frequencies selected for this work, velocity profiles were extracted at two stations ($x/c = 0.4$, $z/c = 0.5$) and ($x/c = 0.4$, $z/c = 0.7$) for four phase angles ϕ of 0, 90, 180, and 270 deg. The velocity profiles at phase angles of 0 and 270 deg reveal a fully attached flow at all spanwise and chordwise

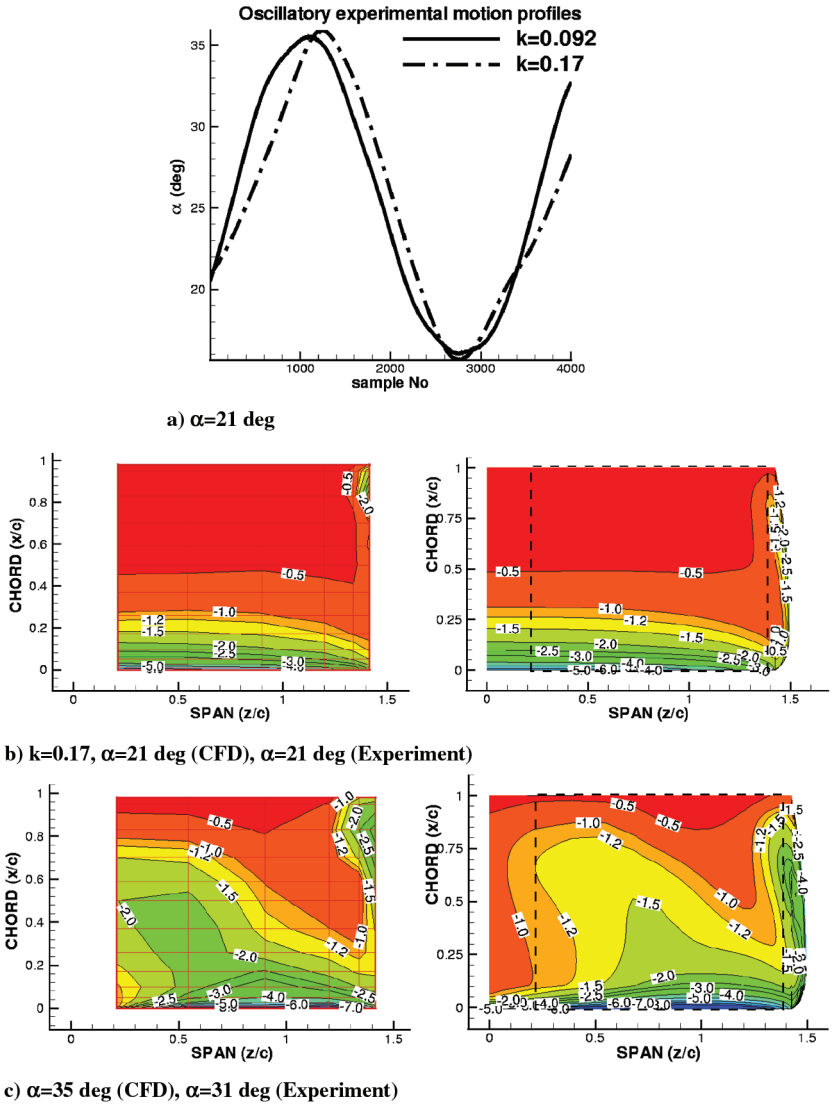

Fig. 7 a) Geometric angle vs sample number of the wing motion for the case by Coton and Galbraith [10]. Oscillatory cases at $k = 0.092$ and $k = 0.17$. b–c) Comparison between experimental (left) and CFD (right) surface pressure distributions for case 4 of Table 1. Oscillating wing motion between 15 and 35 deg, $Re = 1.5 \times 10^6$, $M = 0.16$, $k = 0.17$.

stations. In contrast, the velocity profiles at 90 and 180 deg show massive recirculation of the flow. This can also be seen from the embedded plots at Figs. 3 and 4.

Overall, the CFD solution predicted the onset and the extend of the separation very well. It is also interesting that the CFD results predict very well the velocity profiles at the outboard station of $z/c = 0.7$ for all phase angles and employed reduced frequencies. As will be discussed in subsequent paragraphs, the flow near the tip is highly 3-D due to the interaction between the DSV and the tip vortex.

C. Pressure Measurements of Coton and Galbraith [10]

The tests described here [10] were carried out in the Handley–Page wind tunnel of the University of Glasgow, which is of low-speed, closed-return type. The planform of the wing model used for this experiment is shown in Fig. 1a. The model had a chord length of 0.42 m, a span of 1.26 m, and was mounted horizontally in the tunnel's octagonal cross section of 2.13×1.61 m. In contrast to other experimental investigation where half-span models were used, Coton and Galbraith [10] used a full-span model with rounded tips. Their model was instrumented with a series of 180 pressure taps grouped in six spanwise locations. In addition, a set of 12 taps was located closer to the tip region. All signals were fed to a data-logging system, at sampling frequencies ranging from 218 to 50,000 Hz, depending on the speed of the wing motion of each case. The experimental data used for this work are averaged from a number of consecutive cycles.

For the CFD investigation, both ramping and oscillatory cases have been selected from the database provided by Coton and Galbraith [10]. Figure 5a presents the time history of the geometric incidence as recorded during the experiment. As can be seen, the idealization of the ramping profile $\alpha = \alpha_o + \dot{\alpha}t$ usually employed in CFD calculations is far from satisfactory. In the present work, the time history of the incidence had to be curve fitted and then sampled according to the desired timestep for each calculation. Several ramping cases have computed, and results are presented here for two cases. Both cases were computed at the same Reynolds and Mach numbers of 1.5×10^6 and 0.16, respectively. The corresponding reduced pitch rates were $\alpha^+ = 0.011$ and 0.022. For both cases the incidence was varied between -5 and 39 deg.

Figure 7a suggests that a similar treatment is required for the oscillatory cases. The ideal case $\alpha = \alpha_o + \alpha_1 \sin(kt)$ had to be generalized so that the imposed wing actuation corresponds the experimental one. It was found that about ten harmonics were necessary and the resulting actuation was described by

$$\alpha = \alpha_o/2 + \sum_{i=1}^{i=10} \alpha_i \sin(ikt) + \beta_i \cos(ikt) \tag{1}$$

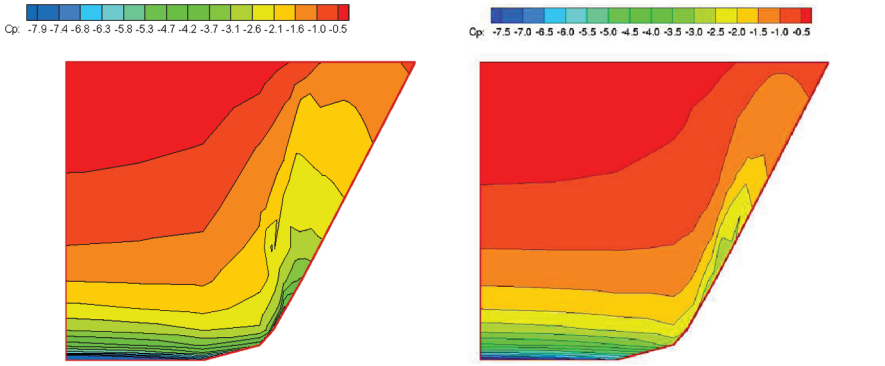

a) α=21 deg (CFD), α=25 deg (Experiment)

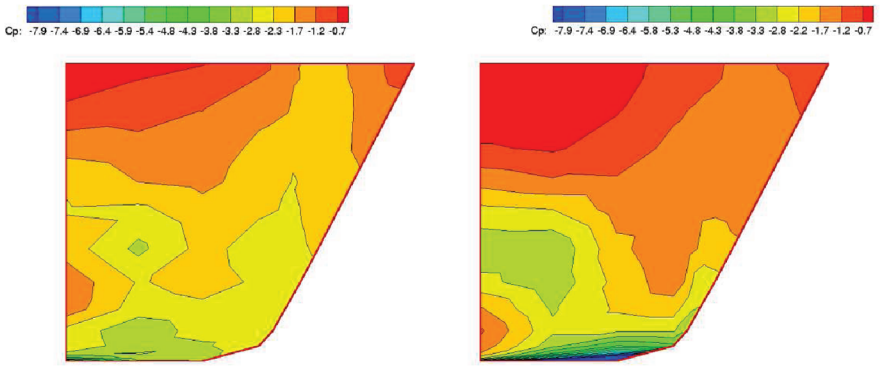

b) α=39 deg (CFD), α=35 deg (Experiment)

Fig. 8 Comparison between experimental (left) and CFD (right) surface pressure distributions for case 5 of Table 1 [10] for the wing with swept-back tips. Oscillating wing motion between 15 and 35 deg, $Re = 1.5 \times 10^6$, $M = 0.16$, $k = 0.17$.

Table 4 presents the bias α_o as well as the amplitudes of the in- and out-phase components used for the CFD simulations.

To allow comparisons with the ramping cases, the Reynolds and Mach numbers were kept the same. Again, two reduced frequencies were used as fundamental harmonics of the oscillation, namely, $k = 0.092$ and 0.17. Comparisons between experiments and CFD results for the surface pressure coefficient are presented in Figs. 5 and 6 for the ramping and Fig. 7 for the oscillatory case.

One cannot fail to notice that at low incidence (20 deg in Fig. 5b), the experiments and CFD agree quite well. The shape of the C_p contours corresponds to attached flow and the suction peak near the leading edge as well as the pressure recovery along the chordwise direction are adequately captured. Because the wing is loaded, the C_p contours near the tip are distorted due to the presence of the tip vortex. Unfortunately, the number of pressure taps used for the experiment does not allow for detailed comparison in the near tip region. The dashed line on the C_p plot of the CFD solution indicates the area covered by the pressure taps, whereas a grid is shown on the experimental plot that indicates the location of the pressure taps on the wind tunnel model. At higher incidence angles, the agreement between experiments and CFD was less favorable. A correction of the incidence angle of 4 deg was necessary to have a similar loading of the wing. As can be seen in Fig. 5c, both experiments and CFD indicate the presence of a massive vortical structure over the wing. This can be seen near the center of the plot at a spanwise location z/c of 0.75, where a local suction peak is present. As will be discussed in subsequent paragraphs, this peak is due to the DS vortex impinging on the wing surface. At this high incidence, a strong tip vortex dominates the near-tip region of the wing. This is now captured by both experiments and CFD and appears as a secondary suction peak at z/c of about 1.4. This secondary peak corresponds to C_p values of about -3, which is much less than the peak due to the DS vortex, which reaches C_p values of -1.2.

Figure 6 compares the time history of the surface pressure coefficient at four locations on the wing. As can be seen, the initial part of the curves is close for all stations, but discrepancies occur at higher incidence angles. For all cases, the magnitude of C_p is predicted well and the only necessary correction is on the phasing. There are many reasons behind the differences between experiments and CFD. For example, the CFD computations have been performed with freestream conditions at the far field of the computational domain, whereas the real wing model was confined by both tunnel walls and supports. For this test case, the experimentalists reported an upwash of 0.5 deg in the tunnel's test section, possibly attributed to the supporting struts of the wing as well as wall effects. In addition, 2-D work [4] indicated that the employed turbulence model can have a strong influence in the obtained results, especially for cases in which the static stall angle of the wing is exceeded.

Similar remarks can be made for the oscillatory cases for which CFD results are presented in Fig. 7. Comparisons are shown only for a phase angle of 90 deg, which corresponds to the highest incidence encountered during the oscillation. Again the suction peaks induced by the DS and the tip vortices are predicted at almost the same magnitude and location.

A separate set of calculations has been conducted for the swept tip planform, which was tested at almost the same conditions as the square wing. Results for this case are shown in Fig. 8, again at two incidence angles. For this case, a similar number of pressure taps was used, and the CFD solution was supplied at the locations of these taps. The data were subsequently used to reconstruct the pressure field in exactly the same way as the experiments. A 4 deg incidence correction had to be applied for the wing loading of the CFD to match the experiment; however, the predicted surface pressure distributions and the location of the DSV and tip vortices were very similar, with the DSV formed further inboard of the tip, in comparison to the straight-tip cases.

D. Experiments by Piziali [12]

The experiments by Piziali have been used by several authors in their studies of 2-D DS. Regardless of their popularity, Ekaterinaris [8] was the only author who attempted the calculation of the 3-D

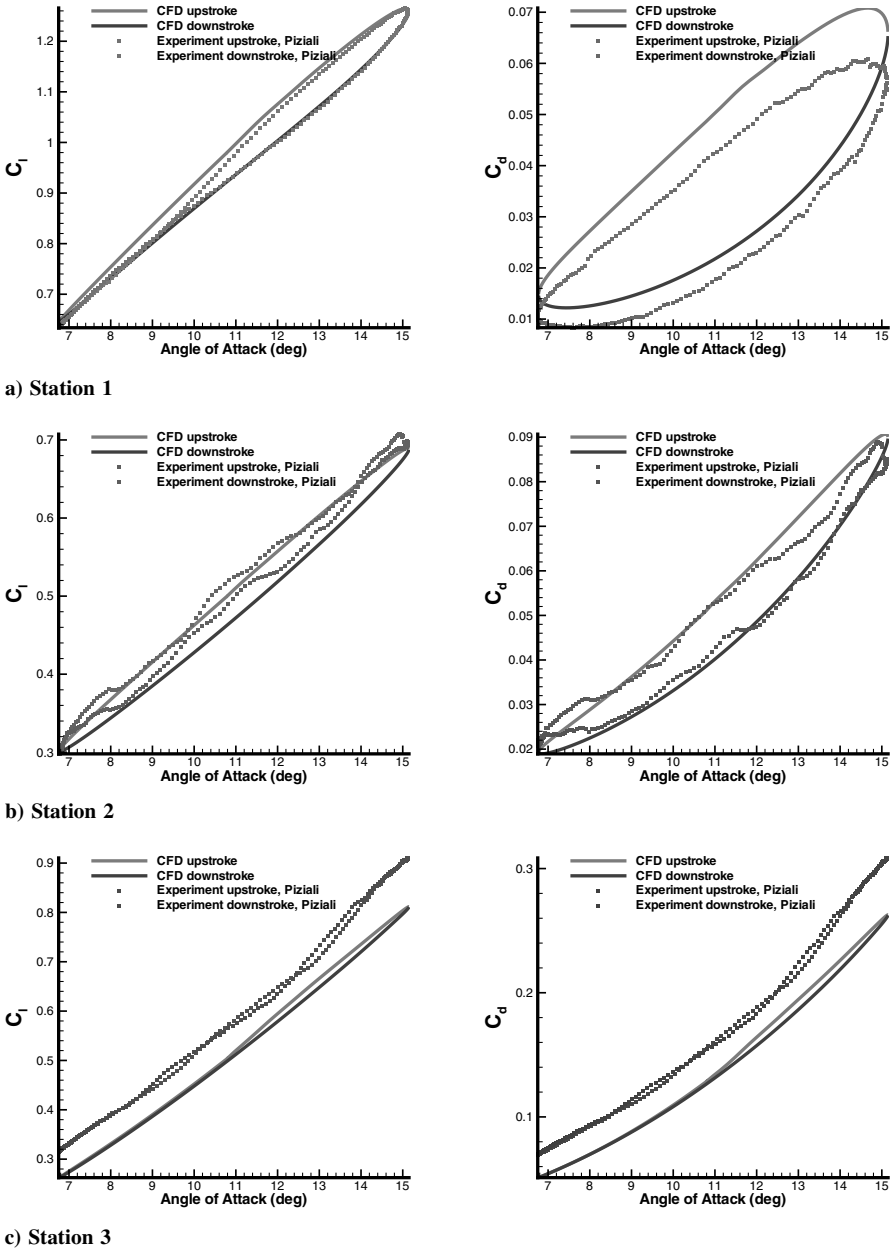

Fig. 9 Comparison between experimental and CFD hysteresis loops for the sectional loads at three stations a) $z/s = 0.47$, b) $z/s = 0.966$, and c) $z/s = 0.995$. The conditions correspond to run r0329 of Piziali [12]. Oscillating wing motion between 7 and 15 deg, $Re = 2.0 \times 10^6$, $M = 0.3$.

case. The case considered by Ekaterinaris has also been used in this work and is an oscillatory motion with a mean angle of 11 deg, amplitude of 4.2 deg, and reduced pitch rate $k = 0.096$.

For his 3-D experiments, Piziali [12] used a small number of spanwise stations equipped with pressure transducers, and reduced the pressure measurements at each spanwise station to sectional coefficients of lift, moment, and drag. The data gathered during numerous oscillations were averaged in time. Figure 9 presents the comparison between CFD and Piziali's data. For this case, the stall angle is slightly exceeded and the inboard part of the wing experiences mild DS. As can been seen from the lift loop at the inboard wing sections, the c_l and c_d of the upstroke part of the motion are higher than that of the downstroke motion. At the same time, the hysteresis of the c_d coefficient is much larger than that of the c_l. As the tip is approached, the hysteresis loops of both the c_l and c_d coefficients become narrow, indicating the influence of the tip vortex, which dominates in the near-tip region and whose characteristics depend primarily on the angle of attack of the wing.

Towards the tip, the flow remains attached and this is shown by the much thinner hysteresis loop. The agreement between CFD and experiments remains favorable up to the last station with a mild shift of the CFD results towards lower lift. It has to be noted that near the tip, the wing model had a support structure, which has not been included in the CFD model and which might have an effect to the quality of the near-tip measurements. Closer examination of the outboard loops indicates that the shift between the CFD results and the experiments is of the order of 1 deg, which could also be attributed to wing flexing as documented by Piziali [12].

IV. Investigation of Flow Topology

Having obtained a flowfield similar to the one indicated by the flow visualization of Moir and Coton [9] and having established confidence on the prediction of the velocity [11,18] and surface pressure fields [10] during 3-D DS, emphasis is now placed on the analysis of the obtained results and the evolution of the flowfield. To complement the calculations conducted so far, an additional case had been studied. For this case no experimental data were available for comparisons. A wing of aspect ratio ten and a linear twist of -10 deg was considered. Since all previous calculations were conducted for

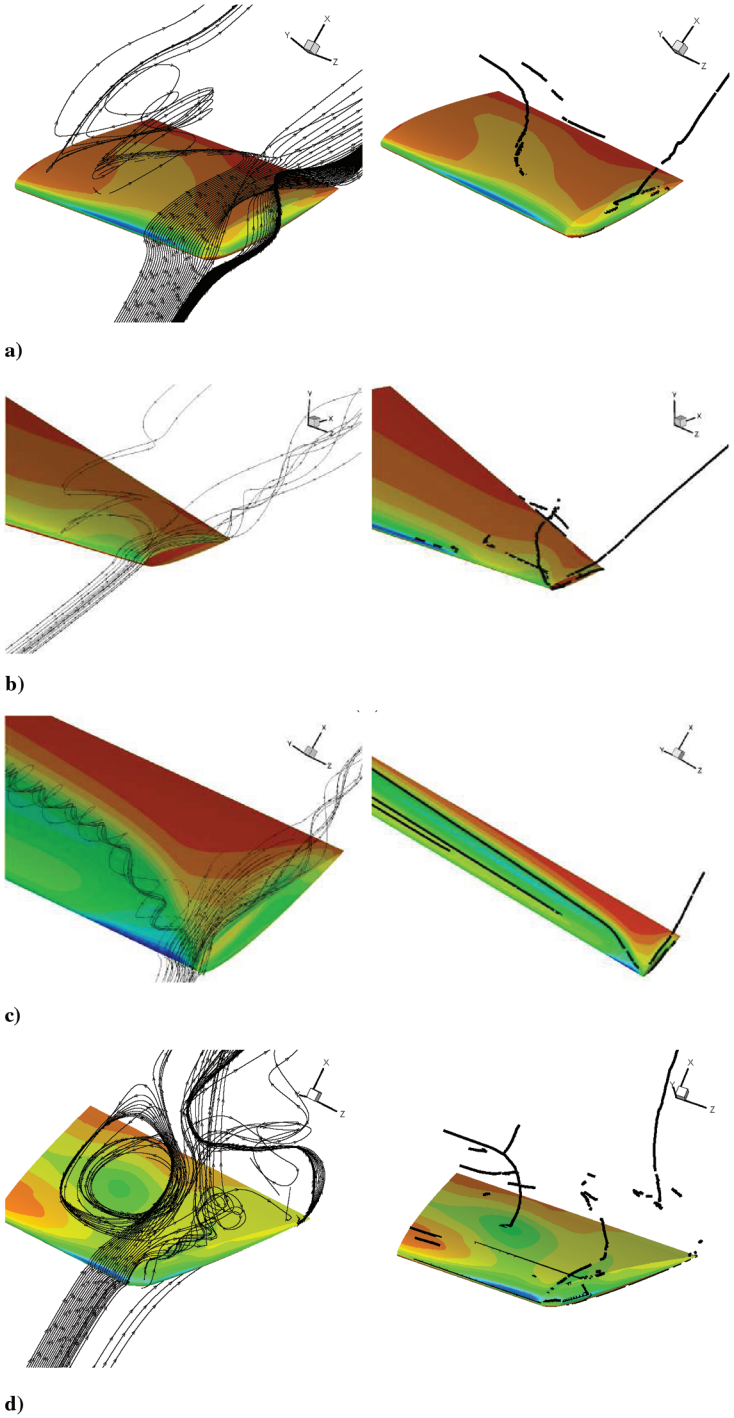

Fig. 10 Streamlines (left) and vortex cores (right) near the stall angle. a) Low aspect ratio wing with rounded tips [10], ramping motion between $\alpha = -5$ and 39 deg, $\alpha^+ = 0.022$, $Re = 1.5 \times 10^6$, $M = 0.16$; b) tapered wing with flat tip [11], oscillatory motion, $k = 0.17$, $Re = 1.5 \times 10^6$, $M = 0.16$; c) large aspect ratio wing with 10 deg negative twist and flat tip, ramping motion between $\alpha = 0$ and 40 deg, $Re = 13,000$, $M = 0.16$, $\alpha^+ = 0.1$; d) swept-back tip by Cotton and Galbraith [10].

low-aspect-ratio wings, it was expected that the evolution of dynamic stall would be quite different for wings of higher aspect ratio. Surprisingly, this was not the case.

Dynamic stall starts with the production of a large vortical structure which is energized by both the freestream and the motion of the wing. Figure 10 shows the streamlines and the vortex cores detected near the stall angle for all planforms considered in this work. In all cases shown, the inboard portion of the DS vortex appears to be parallel to the trailing edge, whereas its outboard portion approaches the leading-edge part of the tip. However, one distinctive difference has been observed for the low-aspect-ratio wing with rounded tips (Fig. 10a). For this case, the DS vortex was terminated inboard of the wing tip in the region where it impinged on the wing surface. This was not the case for the high aspect ratio and the tapered wings (Figs. 10b and 10c) where the DS vortex appears to be closer to the tip vortex near the leading edge of the wing. The same configuration with the DS vortex impinging almost vertically on the wing (Figs. 10a and 10d) was observed in Fig. 2. This was also observed by the authors in previous investigations [16,17] where the DS of low aspect ratio wings was studied. By far the most interesting configuration can be seen in Fig. 10d, in which a very complex vortical structure is encountered. The DSV appears to hit the wing's surface further inboard of the tip and the tip vortex develops an almost spiral structure and dominates the region near the tip but also

further inboard. Thinking along the lines of the vortex theorems of Helmholtz, the observed configurations seem valid, as vortices either extend to infinity, merge with other vortices, or end on solid surfaces.

V. Conclusions

Detailed validation of a CFD method has been undertaken for 3-D dynamic stall cases. For the laminar test cases, all flow structures identified with smoke visualization were present in the CFD solutions, and the flow topology was found to be predicted with remarkable precision.

Moving to high Reynolds number flows, the velocity profiles on the tapered-wing case of the Laboratory of Marseille [11] were predicted extremely well at all phase angles and all spanwise locations where measurements were available. The more demanding cases by Coton and Galbraith [10] were predicted reasonably well with some discrepancies in the stall angle.

The most remarkable conclusion of this work is the almost universal configuration obtained for the 3-D DSV and the tip vortex for all planforms investigated. It appears that the tip and the Ω-shape vortex form a Π-Ω configuration regardless of the planform shape, provided of course that conditions for dynamic stall are achieved.

Several issues remain to be investigated and consequently some future steps must be undertaken. These include the investigation of the turbulence modeling and simulation aspects of the current CFD solver and the identification of the most promising technique for turbulent flow simulations. Calculations are currently underway with detached eddy simulation as well as large eddy simulation to reveal limitations, if any, in the RANS approach employed in this work. The effect of flow transition also merits a separate investigation.

Acknowledgment

Financial support from the Engineering and Physical Sciences Research Council (EPSRC) (Grant GR/R79654/01) is gratefully acknowledged.

References

[1] Ekaterinaris, J. A., Srinivasan, G. R., and McCroskey, W. J., "Present Capabilities of Predicting Two-Dimensional Dynamic Stall," *Aerodynamics and Aeroacoustics of Rotorcraft*, AGARD Conference Papers CP-552, AGARD, Aug. 1995.

[2] Ekaterinaris, J. A., and Platzer, M. F., "Computational Prediction of Airfoil Dynamic Stall," *Progress in Aerospace Sciences*, Vol. 33, Nos. 11–12, 1997, pp. 759–846.

[3] Visbal, M. R., "Effect of Compressibility on Dynamic Stall of a Pitching Aerofoil," AIAA Paper 88-0132, Jan. 1988.

[4] Barakos, G. N., and Drikakis, D., "Computational Study of Unsteady Turbulent Flows Around Oscillating and Ramping Aerofoils," *International Journal for Numerical Methods in Fluids*, Vol. 42, No. 2, 2003, pp. 163–186.

[5] Newsome, R. W., "Navier-Stokes Simulation of Wing-Tip and Wing-Juncture Interactions for a Pitching Wing," AIAA Paper 94-2259, June 1994.

[6] Schreck, S. J., and Helin, H. F., "Unsteady Vortex Dynamics and Surface Pressure Topologies on a Finite Wing," *Journal of Aircraft*, Vol. 31, No. 4, 1994, pp. 899–907.

[7] Morgan, P. E., and Visbal, M. R., "Simulation of Unsteady Three-Dimensional Separation on a Pitching Wing," AIAA Paper 2001-2709, June 2001.

[8] Ekaterinaris, J. A., "Numerical Investigation of Dynamic Stall of an Oscillating Wing," *AIAA Journal*, Vol. 33, No. 10, 1995, pp. 1803–1808.

[9] Moir, S., and Coton, F. N., "An Examination of the Dynamic Stalling of Two Wing Planforms," Univ. of Glasgow, G.U. Aero. Rept. 9526, Glasgow, Scotland, 1995.

[10] Coton, F. N., and Galbraith, R. A. M., "An Experimental Study of Dynamic Stall on a Finite Wing," *The Aeronautical Journal*, Vol. 103, No. 1023, 1999, pp. 229–236.

[11] Berton, E., Allain, C., Favier, D., and Maresca, C., "Experimental Methods for Subsonic Flow Measurements," *Progress in Computational Flow-Structure Interaction*, edited by W. Haase, V. Selmin, and B. Winzell, Vol. 81, Notes on Numerical Fluid Mechanics and Multidisciplinary Design, Springer, New York, 2003, pp. 97–104.

[12] Piziali, R. A., "2-D and 3-D Oscillating Wing Aerodynamics for a Range of Angles of Attack Including Stall," NASA TM-4632, Sept. 1994.

[13] Tang, D. M., and Dowell, E. H., "Experimental Investigation of Three-Dimensional Dynamic Stall Model Oscillating in Pitch," *Journal of Aircraft*, Vol. 32, No. 5, 1995, pp. 163–186.

[14] Badcock, K. J., Richards, B. E., and Woodgate, M. A., "Elements of Computational Fluid Dynamics on Block Structured Grids Using Implicit Solvers," *Progress in Aerospace Sciences*, Vol. 36, Nos. 5–6, 2000, pp. 351–392.

[15] Wilcox, D. C., "Reassessment of the Scale-Determining Equation for Advanced Turbulence Models," *AIAA Journal*, Vol. 26, No. 11, 1988, pp. 1299–1310.

[16] Spentzos, A., Barakos, G., Badcock, K., Richards, B., Wernert, P., Schreck, S., and Raffel, M., "Investigation of Three-Dimensional Dynamic Stall Using Computational Fluid Dynamics," *AIAA Journal* Vol. 34, No. 5, 2005, pp. 1023–1033.

[17] Spentzos, A., Barakos, G., Badcock, K., Richards, B., Wernert, P., Schreck, S., and Raffel, M., "CFD Investigation of 2D and 3D Dynamic Stall," *AHS 4th Decennial Specialist's Conference on Aeromechanics* [CD-ROM], Paper 2-4, Jan. 2004.

[18] Berton, E., Allain, C., Favier, D., and Maresca, C., "Database for Steady and Unsteady 2-D and 3-D Flow," *Progress in Computational Flow-Structure Interaction*, edited by W. Haase, V. Selmin, and B. Winzell, Vol. 81, Notes on Numerical Fluid Mechanics and Multidisciplinary Design, Springer, New York, 2003, pp. 155–164.